accepted for publication in the Astrophysical Journal, 1999

Obscuration of the Parsec Scale Jets in the Compact Symmetric Object 1946+708

A. B. Peck[1,2], G. B. Taylor[1], J. E. Conway[3]

ABSTRACT

We present results of VLA and VLBA observations of the 1.420 GHz neutral hydrogen absorption associated with the Compact Symmetric Object 1946+708 (z=0.101). We find significant structure in the gas on parsec scales. The peak column density in the H I ($N_{\rm HI} \simeq 2.2\times10^{23}$ cm^{-2}($\frac{T_s}{8000{\rm K}}$)) occurs toward the center of activity of the source, as does the highest velocity dispersion ($\Delta V_{\rm FWHM} \simeq$350 km s^{-1}). In addition, we find that the continuum spectra of the various radio components associated with these jets strongly indicate free-free absorption. This effect is particularly pronounced toward the core and inner components of the receding jet, suggesting the presence of a screen local to the source, perhaps part of an obscuring torus.

Subject headings: galaxies:active – galaxies:individual (1946+708) – radio continuum:galaxies – radio lines:galaxies

[1]National Radio Astronomy Observatory, P.O. Box O, Socorro, NM 87801; apeck@nrao.edu,gtaylor@nrao.edu

[2]Physics Dept., New Mexico Institute of Mining and Technology, Socorro, NM 87801

[3]Onsala Space Observatory, Onsala, S-439992, Sweden

1. Introduction

The radio source 1946+708 is a Compact Symmetric Object (CSO) associated with a m_v=18 galaxy at a redshift of z=0.101±0.001 (Stickel and Kühr 1993). Assuming H_0=75 km s^{-1} Mpc^{-1}, 1 mas corresponds to 1.65 pc.

CSOs are a recently identified class of radio source which are less than 1 kpc in size, and are thought to be very young objects ($\leq 10^4$ yr, Readhead et al 1996a;Owsianik & Conway 1998). These sources are uniquely well suited to investigations into the physics of the central engines, providing in particular a means to test the "unified scheme" of active galactic nuclei (AGN). The unified scheme requires an obscuring region of atomic or molecular gas surrounding the central engine which effectively shields the inner few parsecs of the source from view if the radio axis lies at a large angle to the line of sight (Antonucci 1993).

In compact sources as young as CSOs, it is reasonable to assume that this circumnuclear material is accreting onto, and "feeding", the central engine, and that this process will lead to their eventual evolution into much larger FR II sources (Readhead et al 1996b; Fanti et al 1995). This infalling material is likely to form an accretion disk (Shakura & Sunyaev 1973). The accretion disk will probably be warped to some degree due to radiation pressure (Pringle 1996), and should be predominantly molecular within a range of radii determined by the midplane pressure in the disk (Neufeld & Maloney 1995). This pressure is determined by the X-ray luminosity of the central engine and the shielding column density of hydrogen. In regions where the pressure falls below the critical value, both outside the radius of the molecular region and above and below the plane of the disk, the gas will be largely atomic. Thus it is possible that the "thin disk" called for in the accretion model of Shakura & Sunyaev, and the "obscuring torus" required for unified schemes are parts of the same continuous toroidal structure. We refer to the entire structure as a "torus," although it is not expected to have well defined boundaries. This torus would obscure the central parsecs of sources which happen to be oriented at large angles to the line of sight, resulting in the observed differences between the Type I (quasar, Seyfert 1) and Type II (radio galaxy, Seyfert 2) objects.

CSOs exhibit milliarcsecond scale jets marked by steep spectrum hotspots (Taylor et al 1996). These jets are oriented at large angles to the line of sight, resulting in very little Doppler boosting of the approaching jet (Wilkinson et al 1994). This means that the receding jet can contain up to half of the radio continuum flux density, and thus an obscuring torus should be detectable toward one or both hotspots, and possibly the core (Conway 1996). There are several methods by which it might be possible to detect such a torus. The following are discussed in this paper: Atomic gas (H I - §3.2), molecular gas

(OH - §3.3) and free-free absorption (§3.4). Interpretation of the results follows in §4.

2. Observations and Analysis

The VLA observations were made in C Array on 6 November, 1994. Both the 1.420 GHz H I and 1.667 GHz OH transitions were observed for a total of 20 minutes in 3 snapshots. Subsequently, VLBA observations were made of the H I line on 22 March, 1995 with 2 bit sampling. A single IF with a bandwidth of 8 MHz was observed in 512 channels, resulting in a frequency resolution of 15.6 kHz. This corresponds to a velocity resolution of 4 km s^{-1}. The 8 VLBA antennas capable of observing at 1.286 GHz were used. Amplitude calibration was derived using the measurements of antenna gain and system temperature recorded at each antenna, and refined using the calibrator 3C84 (0316+413). Global fringe fitting was performed using the AIPS task FRING, with a solution interval of three minutes. Considerable attention was paid to the bandpass calibration to eliminate a "slope" which was probably due to the inapplicability of the assumed values of the amplitude calibration signal across the band at this non-standard frequency. Following the standard application of bandpass calibration in AIPS using 3C84, removal of the slope was achieved by applying a second bandpass correction using solutions calculated from the outer 400 line-free channels of 1946+708 itself.

Continuum subtraction for the VLBA data was done in Difmap (Shepherd, Pearson & Taylor 1995) using a model of CLEAN components made from several line-free channels. Subsequent editing and imaging of all data was also done using Difmap. The data were then smoothed to a velocity resolution of 12 km s^{-1}, and the absorption spectra were analyzed using the Groningen Image Processing System (GIPSY; van der Hulst et al 1992) and AIPS.

3. Results

3.1. Radio Continuum

The morphology and orientation of 1946+708 is well understood as a result of a study by Taylor & Vermeulen (1997) in which the proper motions of the jet components were determined. This study used data taken at 3 frequencies over a four year period to measure the rate of increase in angular separation between pairs of jet components. The components were identified from the 8 GHz VLBA radio continuum image from Taylor & Vermeulen (1997) shown in Figure 1a. The rate of expansion between components N2 and S2 was determined to be 0.17 mas/yr or $0.74h^{-1}$c and the resulting range of angles of inclination to the line of sight is θ=65-80°, where the northern side of 1946+708 is the approaching jet.

Figure 1b shows the 1.290 GHz VLBA continuum image. The source components have been labeled as identified in Figure 1a. The core is located halfway between the northern hotspot (NHS) and southern hotspot (SHS), which mark the ends of the approaching and receding jets, respectively. The observations from which the 1.290 GHz image was made suffered a lack of short baselines owing to the inability of the VLBA antennas at KP and FD to observe at this non-standard frequency. Despite this, the total flux densities measured in the VLBA and VLA observations differ by less than 2%, indicating that there is very little radio emission on scales of 100 to 1000 mas.

3.2. H I Absorption

Observations were made at 1.290 GHz, the frequency of the redshifted H I line, with both the VLA and the VLBA. The resulting integrated spectra are shown in Figure 2. The absorption components shown are within the errors of the redshift of the source. The optical depth of the component centered on 1.2913 GHz is very similar in both observations, but the lower frequency component appears to have decreased from $\tau \simeq 0.050\pm.007$ in the VLA observation to $0.035\pm.007$ in the VLBA observation. This difference could be due to 1) an actual change in opacity along the line of sight, 2) the small amount of flux missing from the VLBA observation being absorbed on large scales, or 3) simply to the noise in the data. Given the known expansion velocity of the jets, (0.03 mas in 0.37 yr) it is unlikely that the line of sight to the background continuum has changed sufficiently to cause this difference.

Figure 3 shows the H I absorption profile toward each of 5 regions across the source. The regions correspond to the groups of radio components indicated in Figure 1b. Although there is clear evidence of absorption toward each region, it is unclear how many distinct components are present in each profile. With the exception of the profile toward the northern hot spot (NHS+N1), a single Gaussian function has been fitted to each profile. The optical depths (τ) determined by these fits are presented in Table 1. The systemic velocity obtained from optical observations of both emission and stellar absorption lines (Stickel & Kühr 1993) is 30279±300 km s^{-1}. Thus all of the H I absorption features reported here are within one sigma of the systemic velocity.

In addition to fitting Gaussian functions to the integrated H I absorption profiles in the boxes shown, fits have also been made at each pixel across the source where the continuum level is higher than 50 mJy. In the regions roughly corresponding to the NHS, N1, N2, and N3 components, two Gaussians were fitted as shown in Figure 4. These functions were limited to a maximum FWHM of 160 km s^{-1} centered within 100 km s^{-1} of the velocities shown for NHSa and NHSb in Table 1. The first row of plots in Figure 4 contain the parameters obtained from fits to the 29970 km s^{-1} line. Pixels with a peak signal to noise ratio less than 2 have been blanked. The absorption occurs across all of the continuum source, with velocity centroids ranging from 29950 to 30070 km s^{-1} (Figure 4a). The linewidth distribution shown in Figure 4b indicates a dramatic increase in velocity dispersion toward the inner receding jet (S2+S3), where the FWHM is ∼150 km s^{-1}. The optical depth is fairly uniform ($\tau \sim 0.06$, Figure 4c) with the exception of the steep gradient toward the receding jet where the optical depth rises to 0.18 on the eastern edge. This corresponds to a region of extremely narrow FWHM, and so might be attributable to bad fits to the data.

Due to the relative weakness of the line centered on 30900 km s^{-1}, fits with a peak signal to noise ratio $\geq$ 1.5 have been allowed. These fits appear in the second row in Figure 4. The central velocities are fairly uniform (V∼30070 km s^{-1}) across the portions of 1946+708 toward which this line is present, as are the FWHM ($\Delta V \sim 50$ km s^{-1}) and optical depth ($\tau \sim 0.04$).

3.3. OH Abundance

Figure 5 shows the VLA spectrum centered on 1.514 GHz, the frequency of the redshifted hydroxyl line. The relationship of the optical depth to the abundance of OH along the line of sight is

$$N(OH) \simeq 2.27 \times 10^{14} T_{ex} \tau \Delta V$$

(O'Dea & Baum 1987). The excitation temperature (T_{ex}) of OH in galactic clouds tends to be much less than the kinetic temperature, in most cases between 4 and 8 K (Dickey, Crovisier & Kazés 1981;Turner 1985), so a value of 8 K is adopted. We assume a ΔV of 100 km s^{-1} based on the average H I linewidths. For the upper limit on optical depth of τ ∼0.006 shown, this results in an upper limit on the column density of $1.089 \times 10^{15} \left(\frac{T_{ex}}{8\mathrm{K}}\right) \left(\frac{\Delta V}{100\mathrm{km/s}}\right)$ cm^{-2}.

Although this is not a particularly stringent upper limit, it is consistent with the non-detections of OH in similar sources (i.e. Cygnus A, Conway 1998). A number of theories have been proposed to explain the apparent lack of molecular absorption (Barvainis & Antonucci 1994; Black 1998), but the simplest is that the extended circumnuclear structure referred to as a torus is predominantly atomic (Maloney 1998).

3.4. Radio Continuum Spectra

By tapering a 5 GHz image of 1946+708 taken using the VLBA on 1995 Sept. 3 (Taylor & Vermeulen 1997) we obtained an image with resolution matched to our 1.290 GHz continuum image. These two images were then combined to generate an image of the spectral index distribution across the source (Fig. 6). At either end of the source a steep spectrum is found, reaching $\alpha = -0.99 \pm 0.1$ (where $S_\nu \propto \nu^\alpha$) in the SW hot spot. In the NE hot spot the spectrum is flatter ($\alpha = -0.29$), and at the center of the source and extending across the inner southern jet, the spectral index is quite flat ($\alpha = 0$). These substantial deviations from the expected spectral index of -1 for optically thin synchrotron emission indicate that the radio emission is absorbed at frequencies below $\sim$5 GHz.

The overall spectrum of the nucleus of 1946+708 from single dish observations (Taylor & Vermeulen 1997 and references therein) from 330 MHz to 100 GHz is shown in Fig. 7. From the VLBA observations (this paper and Taylor & Vermeulen 1997) we can study the spectra of groups of components between 1.3 and 15 GHz, though the dramatic change in resolution and (u, v) spacings over this range of frequencies can result in the flux density of some larger components (especially SHS) being underestimated at 8 and 15 GHz. We see that the spectra of the various components differ substantially. Most noteworthy is the inner portion of the receding jet. The spectrum of this group of components (S2 + S3) is fairly steep between 8 and 5 GHz, but flattens dramatically between 5 and 1.3 GHz.

4. Discussion

A number of sources have been discovered which exhibit clear evidence of one or more of the features associated with an obscuring torus. We list a few recent examples. Herrnstein et al (1997) have determined the size and shape of the warped molecular disk in NGC 4258 as traced by maser spots. In this source, the masing disk extends from 0.13 pc to 0.25 pc from the central engine. Evidence of a circumnuclear torus of atomic gas has been seen in Cygnus A and Hydra A. In Cygnus A, H I absorption measurements with the VLBA indicate a torus with a radius of $\sim$50 pc (Conway 1998). In Hydra A, evidence is found for free-free absorption toward the core and inner jets, as well as an H I torus with a scale height of $\sim$30 pc (Taylor 1996).

Additional sources show evidence of a toroidal structure, but the distribution of maser spots or H I absorption is not as well understood. For example, megamasers are also seen in the Circinus galaxy (Greenhill et al 1997), NGC 3079 (Baan & Haschick 1996) and NGC 4945 (Greenhill et al 1997). At least one of these, NGC 3079, also exhibits H I absorption toward the core (Satoh et al 1997). Observations of NGC 1068 suggest evidence of three phenomena, consisting of OH and H_2O masers, H I absorption, and a compact source of free-free emission (Gallimore, Baum & O'Dea 1996). In this source, the maser emission indicates that the molecular disk makes a large angle with the radio axis (Greenhill & Gwinn 1997) and so might be more strongly warped than that of NGC 4258.

Figure 8a shows a cartoon of what the circumnuclear structure could look like. Some notable simplifications have been made. For example, it is not necessary for the toroidal structure to be perpendicular to the jet axis, the "clumps" of denser gas are unlikely to be uniform in size, and the degree of warp in the disk can vary greatly (Maloney 1998). Also, the relative scale heights and radii of the various regions are not very well constrained. This model represents only the central $\leq$100 pc of the source, and does not address the possibility of an extended disk or torus associated with the host galaxy, although this could conceivably be part of the same continuous structure. The extent of the molecular disk is likely to be on the order of a parsec, and the region of atomic gas beyond that probably extends some 50-100 pc from the central engine. This outer region, although predominantly neutral atomic gas, should contain a significant fraction of free electrons (1 - 10%, Maloney, Hollenbach & Tielens 1996), and also probably contains clumps or clouds of denser gas which could harbor molecular gas.

Applying this model to 1946+708, the atomic region in the torus appears to be at least 50 pc in radius and 20 pc in scale height. The free-free absorption is probably due to ionized gas in this torus, and to the central ionized region along the line of sight to the southern, receding jet. Our line of sight to the jet components is shown in Figure 8b.

4.1. The ionized gas

Three of the regions in 1946+708 exhibit a flattening of the continuum spectrum between 1.3 and 5 GHz (Fig. 7); NHS+N1, C+N5+S5, and S2+S3. There are generally two mechanisms invoked to produce such a low frequency turnover in compact extragalactic radio sources: (1) synchrotron self-absorption and (2) free-free absorption by a screen of ionized gas. Under equipartition conditions and for uniformly filled components, synchrotron self-absorption becomes important at GHz frequencies for components with brightness temperatures (T_b) approaching the mean kinetic energy (10^{10} K) of the radiating relativistic electrons (Williams 1963). Thus synchrotron self-absorption is only likely for the northern hot spot (NHS+N1), where $T_b = 4 \times 10^8$ K, and the unresolved core ($T_b > 10^9$ K) in 1946+708. Since the core makes only a minor contribution ($<$ 10 %) to the flux density in the inner parts of the source at 1.3 and 5 GHz, however, it seems likely that free-free absorption is the dominant mechanism for the low frequency turnover in both C+N5+S5 and S2+S3. For a pure H plasma the free-free optical depth is given by:

$$\tau_{\rm ff} \simeq 5 \times 10^{-8}\, T_4^{-3/2}\, n_{\rm e}^2\, \nu_9^{-2}\, g\, d_{\rm pc},$$

(Scheuer 1960;Mezger & Henderson 1967; Levinson, Laor, & Vermeulen 1995) where $d_{\rm pc}$ is the path length through the absorbing medium in parsecs, T_4 is the gas temperature in units of 10^4 K, $n_{\rm e}$ is the electron density in cm^{-3}, ν_9 is the frequency in GHz, and g is the thermal average Gaunt factor. This factor is of order 5 for $T_4 = 1$ and $\nu_9 = 1.3$ (Spitzer 1978). We estimate the expected flux densities at 1.3 GHz for the two free-free absorbed regions based on the observed spectral indices between 5 and 15 GHz. These values are shown in Table 2. The free-free optical depth, column densities, and electron densities are also calculated, assuming a path length of 50 pc through the obscuring material toward C+N5+S5 and S2+S3, and a temperature $T_4 = 0.8$. If the ionized gas is associated with the H I torus, as the distribution of spectral indices in Figure 6 and the high column density toward the inner receding jet suggest, the expected ionized fraction is 1-10% (Maloney et al 1996). The column densities shown in Tables 1 and 2 indicate an ionization fraction around 11% toward the core and 30% toward the inner receding jet. Although these large percentages could be due to incorrect assumptions in the calculation of column densities, this difference could indicate that along the line of sight to S2+S3, the inner receding jet, we are also probing the region between the inner torus and the jet, where the ionization fraction should be much higher.

4.2. The atomic gas

In all profiles except (NHS+N1) shown in Figure 3, there appear to be two or more lines which are very close in velocity or are blended. The top row in Figure 4 shows that single Gaussian functions centered on 30040±70 can be fit to the profiles in almost all regions across the source. This uniformity does not indicate, however, that a single H I feature is present in front of the entire radio continuum source, but rather that when numerous components are present, their velocities straddle this value. This can be seen in the range of ΔV (30-150 km s^{-1}). If the velocity dispersion seen in the profiles is indicative of rotation, this central velocity of 30040±70 km s^{-1} is likely to be the true systemic velocity.

We can compare the H I data from 1946+708 to sources in which we know that the H I absorption is taking place in colder gas in a kpc scale torus or in the host galaxy. In these cases, we see multiple lines along each line of sight, all of which are quite narrow and distinct from one another. In the case of Centaurus A where a kpc scale dust lane intersects our line of sight to the core, at least three H I absorption components are present, each with a FWHM of only 7 to 12 km s^{-1} (van der Hulst, Grolisch & Haschick 1983; Peck & Taylor 1998). Similarly, toward the center of our own Galaxy, Liszt et al (1983) find multiple components with an average FWHM <20 km s^{-1}. In contrast, although there are indications for substructure within the 1946+708 absorption profiles (see Section 3.2), the individual components are considerably broader than those in the galactic or Centaurus A absorption profiles. Furthermore these components, rather than being distinct, are overlapping in velocity. This blending of the absorption lines is probably due to high velocity dispersion between clouds or clumps in a hot medium. These profiles suggest that the HI gas in 1946+708 lies in a considerably more energetic environment, such as that found within a few hundred parsecs of the central engine of an AGN. This model is further supported by variations in the column densities over regions on the order of 10 pc, with the highest values centered on the core of the radio source.

The optical depth is calculated using the integrated line amplitude and the integrated continuum flux within each box outlined in Figure 3. The column density is calculated using

$$N_{\rm HI} \simeq 1.823 \times 10^{18} {\rm cm}^{-2}{\rm K}^{-1}({\rm km/s})^{-1} \times (\tau/f) \times T_s \times \Delta V$$

assuming a covering factor (f) of 1, and a spin temperature (T_s) of 8000 K. Models predict that atomic gas irradiated by hard X-rays should have a stable equilibrium temperature of ~8000 K (Maloney et al. 1996). According to the calculations of Maloney, Hollenbach and Tielens (1996), circumnuclear H I gas becomes self shielding to the hard X-rays which heat it for column densities of 10^{22} cm^{-2} and above. We can therefore ask whether the kinetic temperature of 8000 K can be maintained through such a gas column, and hence whether solutions with this temperature and column density are self-consistent. Clearly the result depends entirely on the (presently unknown) hard X-ray luminosity of 1946+708. However, we can say that if this X-ray luminosity is comparable to that of Cygnus A (which also has a comparable inferred H I column), then for gas which lies within 1 kpc of the central engine, the X-ray heating would be sufficent to keep all of the H I column at 8000 K (Blanco & Conway 1996, Conway & Blanco 1995). Although there might also be cooler gas present at the interface between the molecular gas and H I in the dense clumps within the torus, the lack of molecular absorption lines suggests that the covering factor of these dense clouds is quite small, and therefore the contribution to the overall H I absorption from these regions would be negligible.

Given an assumed distance of 100 pc from the central engine, the inferred H I column density (assuming T_s = 8000 K and a maximum atomic gas filling factor of unity) implies a neutral hydrogen density of $n_{\rm HI}$ ~8×10^2 cm^{-3}. At this distance, given the source radio flux density, the increase in spin temperature due to radiative excitation should be less than

15% (Bahcall & Ekers 1969). Hence the assumption that the spin temperature is about equal to the kinetic temperature is self consistent in our modelling and we will assume this in our calculations.

The regions of peak absorption intensity toward the northern hotspot are separated by $\sim$2 mas ($33h^{-1}$ pc). It seems unlikely that this could be due to the rotation of gas in a circumnuclear torus, because it would indicate that the torus is offset by 30° from the radio axis, rather than the expected 90°, and that the inner radius of the torus has a velocity of only 65 km s^{-1}. The offset of the peaks of these two lines is more likely to be due to the presence of "clumps" in the toroidal structure surrounding the central engine. These narrow lines could be dense compact regions of H I in the host galaxy, and not associated with the AGN, though they are still substantially broader than typical galactic H I absorption lines.

The high column density and velocity dispersion of the gas toward the core is more indicative of a rotating torus. The signal to noise ratio in the present observations was not high enough to determine the spatial offset between the outermost velocity components, and so the simplest model of a torus perpendicular to the radio axis is assumed. Given that the high opacity region covering the core is less than 50 pc in height, and that the broad absorption covers much of the counterjet which is at 65-80° to the line of sight, the obscuring torus is probably at an angle of order 20° from edge-on with a radius of at least 50 pc (see Figure 8b). Assuming gravitationally bound gas, possibly in rotation, and a relatively thick disk able to cover both the counterjet and the core, then the dispersion velocity along the line of sight must be comparable to the rotational velocity or total random velocity within the disk. The 350 km s^{-1} FWHM of the gas at 25−50 pc then implies, from rough virial arguments, a central mass of M$\sim 5\times10^8$ M$_\odot$. Without a detailed model, this estimate is highly uncertain, but it is consistent with the central masses inferred in active galactic nuclei by other methods.

5. Conclusion

Neutral hydrogen is present toward all of the radio components in the Compact Symmetric Object 1946+708. Narrow lines seen toward the northern hotspot which marks the approaching jet are probably due to small clouds of H I associated with an extended "clumpy" torus of warm gas. The high velocity dispersion and column density toward the core of the source, however, are indicative of fast moving circumnuclear gas, perhaps in a rotating toroidal structure. Further evidence for this region of high kinetic energy and column density is found in the spectra of the jet components, which indicate a region of free-free absorption along the line of sight toward the core and inner receding jet. The most likely scenario to explain these phenomena consists of an ionized region around the central engine, surrounded by an accretion disk or torus with a radius of at least 50 pc which is comprised primarily of atomic gas.

The authors thank the referee, Jack Gallimore, and Miller Goss for helpful suggestions and discussion. The National Radio Astronomy Observatory is a facility of the National Science Foundation operated under a cooperative agreement by Associated Universities, Inc. AP is grateful for support from NRAO through the pre-doctoral fellowship program. This research has made use of the NASA/IPAC Extragalactic Database (NED) which is operated by the Jet Propulsion Laboratory, California Institute of Technology, under contract with the National Aeronautics and Space Administration.

REFERENCES

Antonucci, R. 1993, ARA&A, 31, 473

Baan, W. A. & Haschick, A. 1996, ApJ, 473, 269

Bahcall, J. N. & Ekers, R. D. 1969, ApJ, 157, 1055

Barvainis, R. & Antonucci, R. 1994, AJ, 107, 1291

Black, J. H. 1998, in *The Molecular Astrophysics of Stars and Active Galaxies*, eds. D. A. Williams and T. W. Hartquist, [Oxford Univ. Press], in press

Blanco, P. R. & Conway, J. E. 1996, in *Cygnus A–Study of a Radio Galaxy*, eds. C.L.Carilli, D.E.Harris [Cambridge Univ. Press], 69

Conway, J. E. 1996, in *The Second Workshop on Gighertz Peaked Spectrum and Compact Steep Spectrum Radio Sources*, eds. I. A. G. Snellen, R. T. Schilizzi, H. J. A. Rottgering and M. N. Bremer [Leiden Observatory], 198

Conway, J. E. 1998, in *Radio Emission from Galactic and Extragalactic Compact Sources*, ASP Conference Series, Volume 144, IAU Colloquium 164, eds. J.A. Zensus, G.B. Taylor, & J.M. Wrobel, p. 231

Conway, J. E. & Blanco P. R. 1995, ApJ, 449, L131

Dickey, J. M., Crovisier, J., & Kazés, I. 1981, A&A, 98, 271

Fanti, C., Fanti, R., Dallacasa, D., Schilizzi, R. T., Spencer, R. E. & Stanghellini, C. 1995, A&A, 302, 317

Gallimore, J. F., Baum, S. A. and O'Dea, C. P. 1996 ApJ 464 198

Greenhill, L. J., Moran, J. M. & Herrnstein, J. R. 1997, ApJ, 481, L23

Greenhill, L. J., Ellingsen, S. P., Norris, R. P., Gough, R. G., Sinclair, M. W., Moran, J. M. & Mushotzky, R. 1997, ApJ, 474, L103

Greenhill, L. J. & Gwinn, C. R. 1997, Ap&SS, 248, 261

Herrnstein, J. R., Moran, J. M., Greenhill, L. J., Diamond, P. J., Miyoshi, M., Nakani, N., Inoue, M. 1997, ApJ, 475, L1

van der Hulst, J. M., Terlouw, J. P., Begeman, K. G., Zwitser, W., & Roelfsma, P. R. 1992, in ASP Conf. Ser., 25, Astronomical Data Analysis Software and Systems I, ed. D.M. Worral, C. Biemesderger, & J. Barnes [San Francisco: ASP], 131

van der Hulst, J. M., Grolisch, W. F. & Haschick, A. D 1983, ApJ, 264, L37

Levinson, A., Laor, A., & Vermeulen, R.C. 1995, ApJ, 448, 589

Liszt, H. S, van der Hulst, J. M., Burton, W. B & Ondrechen, M. P. 1983, A&A, 126, 341

Maloney, P. R. 1998, in *Highly Redshifted Radio Lines*, eds C. Carilli, S. Radford & G. Langston, ASP, *in press*

Maloney, P. R., Hollenbach, D. J. & Tielens, A. G. G. M. 1996, ApJ, 466, 561

Mezger, P. G. & Henderson, A. P. 1967, ApJ, 147, 471

Neufeld, D. A. & Maloney, P. R. 1995, ApJ, 447, L17

O'Dea, C. P. & Baum, S. A. 1987, AJ, 94, 1476

Owsianik, I. & Conway, J. E. 1998, AA, 337, 690

Peck, A. B. & Taylor, G. B. 1998, BAAS, 193, 620

Pringle, J. E. 1996, MNRAS, 281, 357

Readhead, A. C. S., Taylor, G. B, Xu, W., Pearson, T. J., Wilkinson, P. N. & Polatidis, A. G. 1996a, ApJ, 460, 612

Readhead, A. C. S., Taylor, G. B, Pearson, T. J., & Wilkinson, P. N. 1996b, ApJ, 460, 634

Satoh, S., Inoue, M., Nakai, N., Shibata, K. M., Kameno, S., Migenes, V., Diamond, P. J. 1997, in *The Central Regions of the Galaxy and Galaxies*, IAU Symposium 184, p. 208

Shakura, N. I. and Sunyaev, R. A. 1973, A&A, 24, 337

Scheuer, P. A. G. 1960, MNRAS, 120, 231

Shepherd, M. C., Pearson, T. J., Taylor, G. B. 1995, BAAS, 27, 903

Spitzer, L. 1978 *Physical Processes in the Interstellar Medium*,(New York:Wiley)

Stickel, M. and Kühr, M. 1993, A&AS, 100, 395

Taylor, G. B. 1996, ApJ, 470, 394

Taylor, G. B., & Vermeulen, R. C. 1997, ApJ, 485, L9

Taylor, G. B., Readhead, A. C. S., & Pearson, T. J. 1996, ApJ, 463, 95

Turner B. E. 1985, ApJ, 299, 312

Ueno, S., Koyama, K., Nishida, M., Yamauchi, S. & Ward, M. J. 1994, ApJ, 431, L1

Wilkinson, P. N., Polatidis, A. G., Readhead, A. C. S., Xu, W. & Pearson, T. J. 1994, ApJ, 432, L87

Williams, P. J. S. 1963, Nature, 200, 56

This preprint was prepared with the AAS LaTeX macros v4.0.

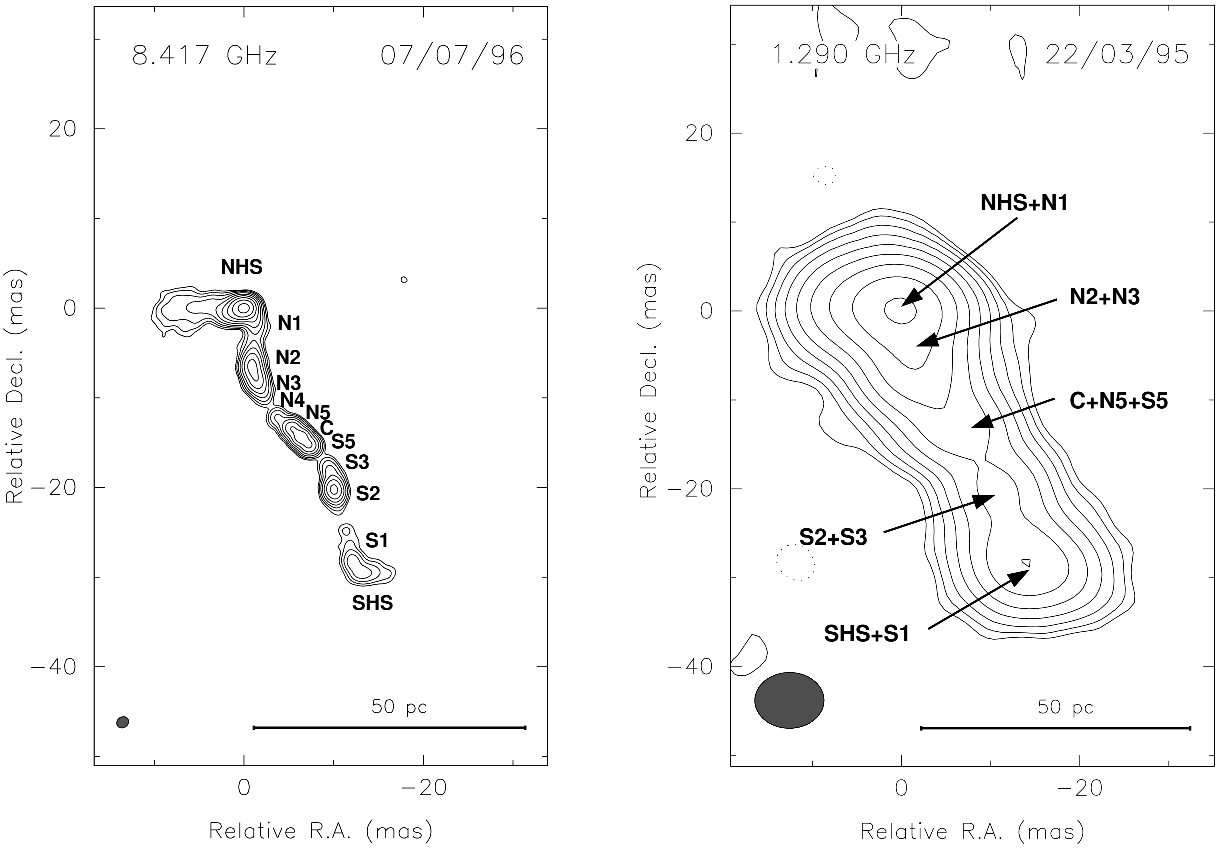

Fig. 1.— 1*a*. Continuum image of 1946+708 at 8.42 GHz. Contours are drawn logarithmically at factor 2 intervals from 0.25 mJy/beam. The beam size is 1.4 $\times$ 1.2 mas with position angle $-55°$. 10 mas is equivalent to $16.5h^{-1}$ pc. NHS and SHS denote the northern and southern hot spots, respectively. The northern side of the jet is the approaching side. 1*b*. Continuum image of 1946+708 at 1.29 GHz. Contours are shown at -2, 2, 4, 8, 16, 32, 64, 128 and 256 mJy/beam. The beam size is 7.8 $\times$ 6.4 mas with position angle 89°. The rms noise in the image shown is 0.7 mJy/beam. The continuum peak is 432 mJy/beam, and the total flux in the source is 1.014 Jy.

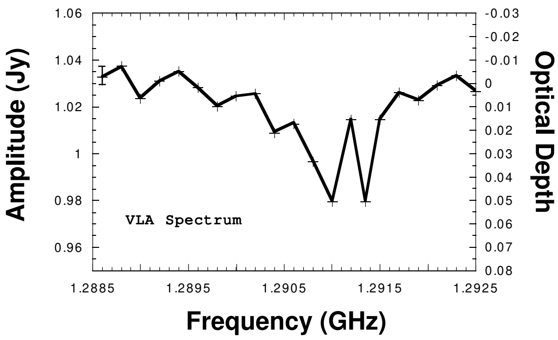

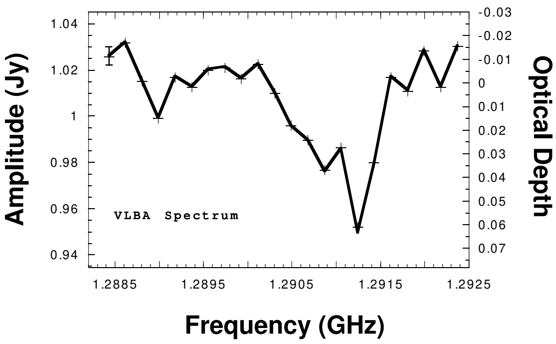

Fig. 2.— VLA and VLBA H I absorption spectra. The first panel shows the VLA spectrum taken in November 1994, in C Array. The second panel shows the integrated spectrum over the entire source taken with the VLBA in March 1995. A typical error bar is shown on the first point in each plot.

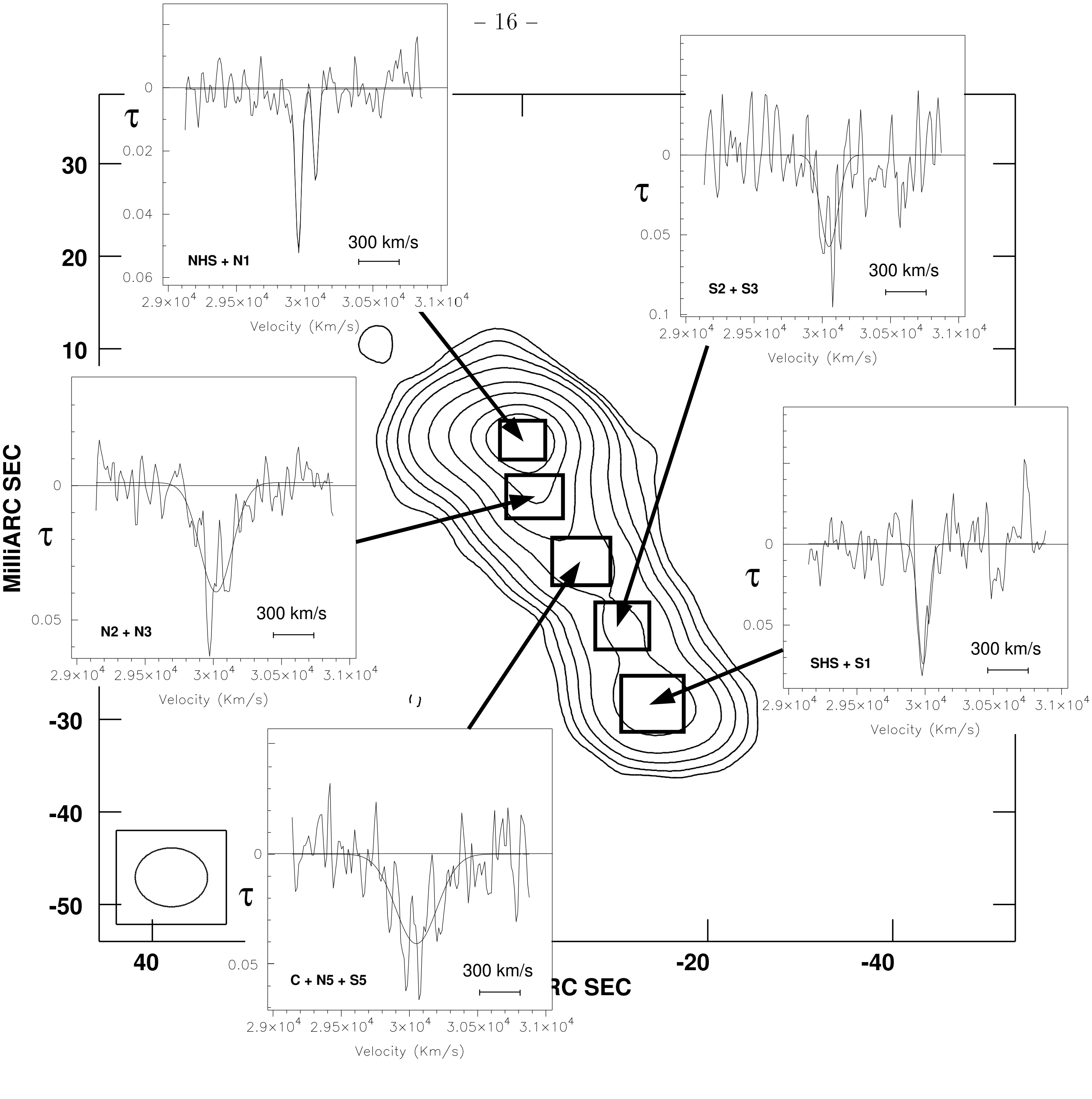

Fig. 3.— Integrated profiles of H I absorption in 5 regions corresponding to radio components identified at 8 GHz in Taylor & Vermeulen (1997). The profile toward the continuum peak (NHS+N1) exhibits two distinct lines separated by 120 km s^{-1}, while the rest contain several blended lines, so two Gaussian functions were fitted to the data in (NHS+N1), and a single Gaussian was fit to each of the other profiles. The data were averaged to 12 km s^{-1} resolution for the Gaussian fits shown, and subsequently Hanning-smoothed to reduce the noise in the plots. The rms noise in the profiles is ~2 mJy/beam/channel.

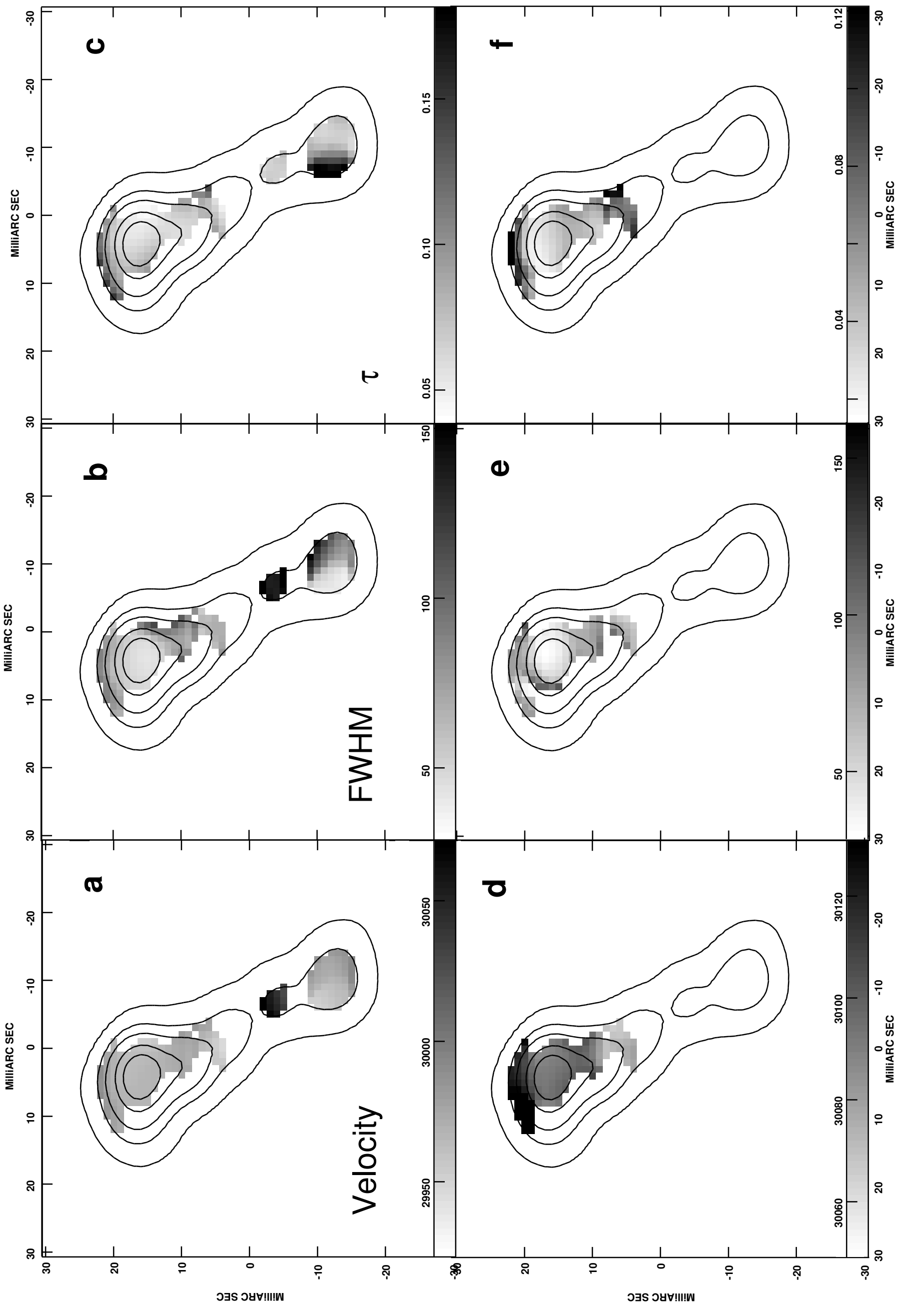

Fig. 4.— The results of Gaussian functions fitted at each pixel where the continuum emission is at least 50 mJy. Grayscale values increase from lighter to darker. Panel 4a shows the velocity field of the line centered on 29970 km s^{-1}. Grayscales range from 29950 to 30070 km s^{-1}. Panel 4b shows the FWHM of the line centered on 29970 km s^{-1}. Grayscales range from 30 to 150 km s^{-1}. Panel 4c shows the optical depth of the 29970 km s^{-1} line. Grayscales range from τ=0.04 to 0.18. Panel 4d shows the velocity field of the line centered on 30090 km s^{-1}. Grayscales range from 30070 to 30150 km s^{-1}. Panel 4e shows the FWHM of the line centered on 30090 km s^{-1}. Grayscales range from 20 to 100 km s^{-1}. Panel 4f shows the optical depth of the 30090 km s^{-1} line. Grayscales range from τ=0.02 to 0.12.

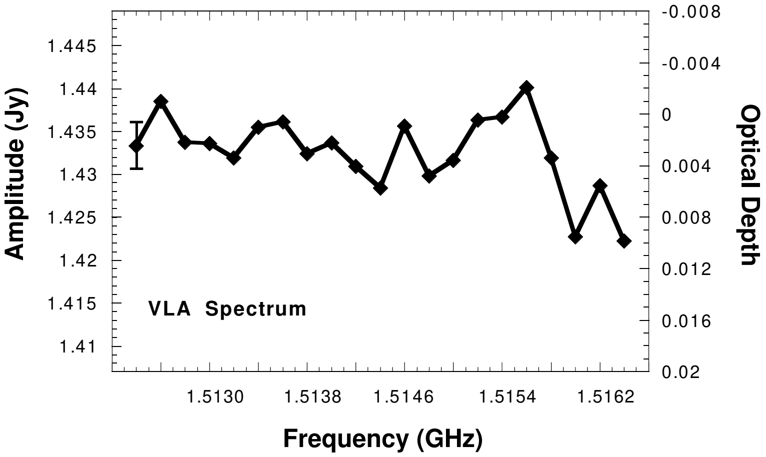

Fig. 5.— VLA spectrum of 1946+708 at 1.514 GHz, the frequency of the OH line at the redshift of z=0.101. A typical error bar is shown on the first point in the plot. The profile shows an upper limit on the OH optical depth of τ=0.006, indicating an upper limit on the OH column density of 1.089×10^{15} cm^{-2}.

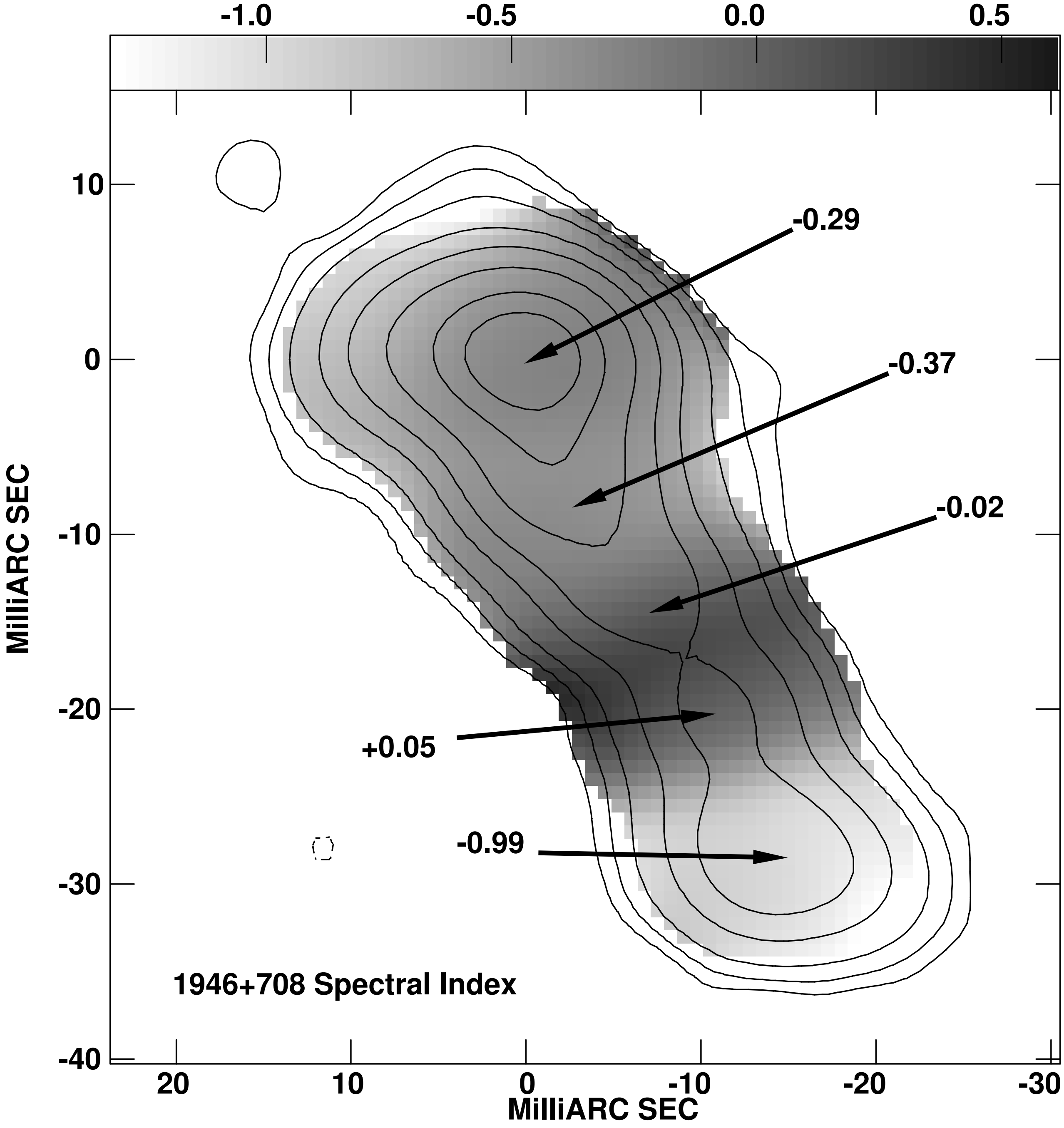

Fig. 6.— Distribution of spectral indices across 1946+708 overlayed on continuum contours, (where $S_\nu \propto \nu^\alpha$). The spectrum flattens substantially toward the core and inner receding jet.

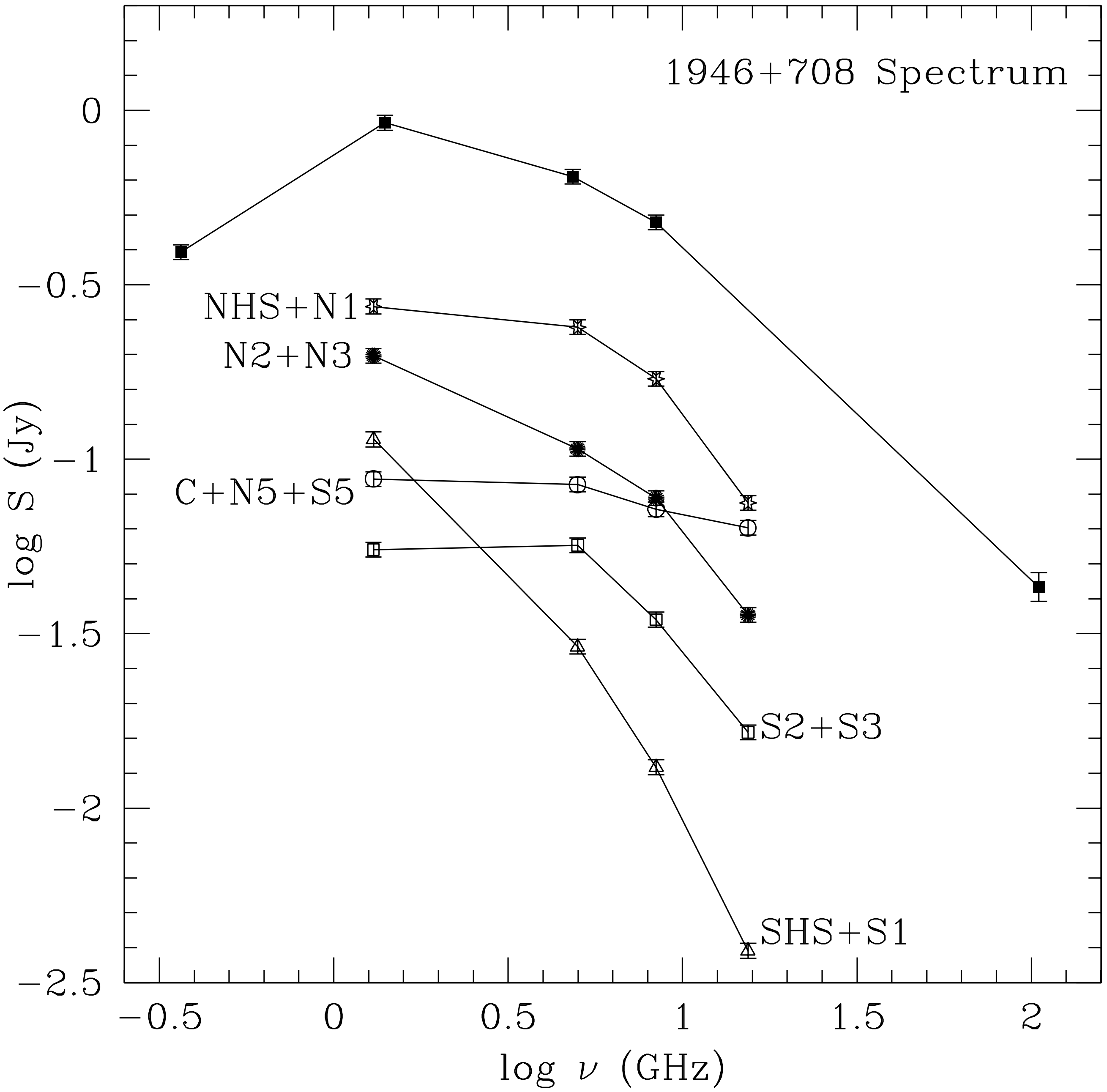

Fig. 7.— Continuum spectra of the various radio components in 1946+708. The spectra of components C+N5+S5 and S2+S3 show clear evidence of free-free absorption, indicating the probable presence of ionized material local to the source.

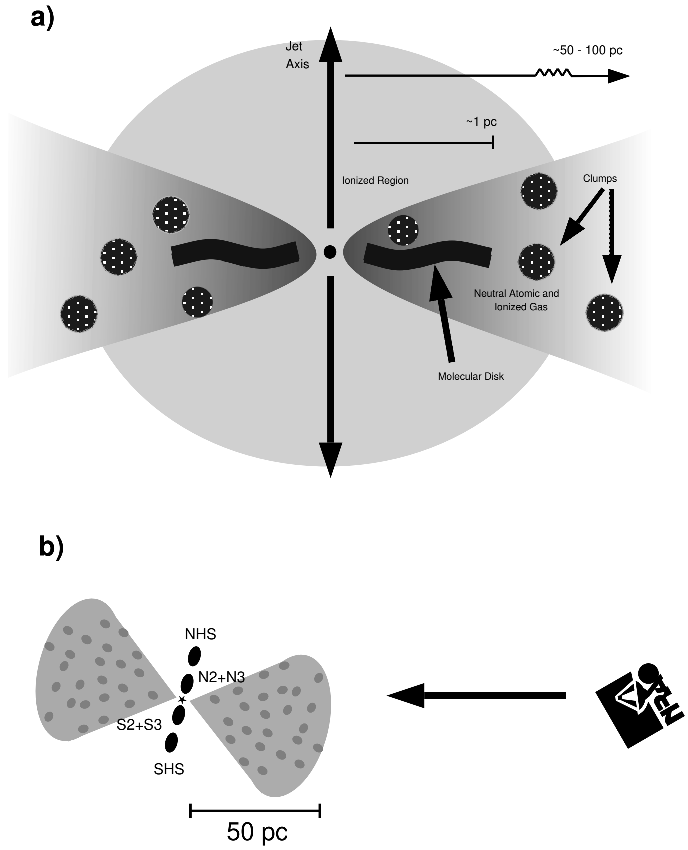

Fig. 8.— a) A cartoon showing the possible environment in the central parsecs of AGN. Some notable simplifications have been made. For example, it is not necessary for the toroidal structure to be perpendicular to the jet axis, the "clumps" of denser gas are unlikely to be uniform in size, and it is believed that the degree of warp in the disk can vary greatly. b) The line of sight to the jet components in 1946+708.

Components	Amplitude (mJy)	Central Velocity (km s^{-1})	FWHM (km s^{-1})	τ	N_{HI}[a] (10^{22} cm^{-2})
NHS+N1a	13.4±2.2	29970±2.5	47.8±5.9	0.057±.009	4.1±0.8
NHS+N1b	7.8±2.4	30090±3.9	40.1±9.3	0.033±.010	2.0±0.7
N2+N3	7.5±1.2	30010±12	273±29	0.041±.006	17±3.0
C+N5+S5	3.8±1.0	30040±23	357±62	0.042±.010	23±6.7
S2+S3	4.8±1.7	30050±16	150±39	0.060±.020	14±5.6
SHS+S1	7.5±2.1	29970±6.9	88.3±17	0.070±.019	11±2.9

Table 1: Gaussian Functions fitted to Absorption Profiles in Each Region

[a]Assuming a spin temperature of 8000 K and a covering factor of 1.

Component	Measured Flux Density	Estimated True Flux Density	τ_{ff}	N_e[a] (cm^{-2})	Density[a] (cm^{-3})
C+N5+S5	88 mJy	126 mJy	0.4	3.0×10^{22}	200
S2+S3	55 mJy	200 mJy	1.3	5.3×10^{22}	350

Table 2: Parameters determined from free-free absorption toward the core and receding jet.

[a]Assuming a temperature of 8000 K and a pathlength of 50 pc.